Immiscible displacements in rough-walled fractures: Competition between roughening by random aperture variations and smoothing by in-plane curvature

Robert J. Glass
Flow Visualization and Processes Laboratory, Sandia National Laboratories, Albuquerque, New Mexico 87185, USA

Harihar Rajaram
Department of Civil, Environmental and Architectural Engineering, University of Colorado, Boulder, Colorado 80309, USA

Russell L. Detwiler
Division of Geophysics and Global Security, Lawrence Livermore National Laboratory, Livermore, California 94551, USA

(Received 18 June 2003; revised manuscript received 3 October 2003; published 31 December 2003)

Phase structure during capillary displacement of fluid phases within rough-walled fractures is controlled by the competition between random aperture variability which tends to roughen the interface and in-plane curvature which tends to smooth it. We show that the phase structure and corresponding areal saturation at the end of displacement depend primarily on the ratio of two dimensionless parameters: one that controls roughening (the coefficient of variation of the aperture field, δ) and another that controls smoothing (the curvature number C, which weighs the mean influences of aperture induced and in-plane curvature). Interestingly, for C/δ above ~ 0.5, areal saturation for wetting and nonwetting invasion first diverges and then converges to create an envelope, whose width increases with δ. This nonunique behavior with respect to wettability is fundamental to capillary displacements in rough-walled fractures and is due to an asymmetry in capillary competition in wetting versus nonwetting invasions.

DOI: 10.1103/PhysRevE.68.061110 PACS number(s): 46.65.+g, 47.55.Mh, 47.55.Kf, 47.54.+r

INTRODUCTION

The general problem of immiscible fluid invasion in disordered porous media has been studied extensively. There, curvature of the phase interface within individual pores is thought to dictate the local capillary forces that drive flow, and in the absence of other forces, variability in pore radii controls phase structure. It is reasonably well established that the invasion percolation (IP) algorithm, which includes only the local pore radius to calculate capillary forces, can reproduce invasion structures found in micromodel experiments for nonwetting fluid invasion [1–3]. Here, the phase interface between immiscible fluids is found to be very rough and has been described as fractal. However, for wetting fluid invasion, the local interfacial curvature is influenced when neighboring pores are also filled with wetting fluid, thus giving rise to a ''dynamic'' effect as invasion proceeds [4,5]. Modifications to the IP algorithm that include this effect have reproduced wetting invasion structure and show significant smoothing of the macroscopic phase interface [6–8].

For phase invasion in rough-walled fractures, several attempts have been made to use the standard IP algorithm by considering the local capillary pressure as calculated from curvature across the local gap or aperture [9–11]. However, geometric arguments suggest that the local curvature is additionally modified by an ''in-plane'' component, reflecting interface curvature in the plane of the fracture. Modifications to the IP algorithm (MIP) to include in-plane curvature have reproduced experimental observations of both wetting and nonwetting invasion [12,8] and have been used in modeling studies of fracture-matrix systems [13]. Importantly, in-plane curvature influences both wetting and nonwetting invasion and can impose significant smoothing of the macroscopic interface. Such smoothing greatly influences the degree (i.e., areal saturation) and nature (i.e., structural complexity) of defending phase entrapment in such a quasi-two-dimensional system and critically controls relative permeability, transport properties and the subsequent dissolution of the entrapped phase [14,15]. The competition between aperture-induced curvature that produces complicated structure and the smoothing influence of in-plane curvature can yield behavior that ranges from the IP limit where entrapment is significant and ramified to near piston displacement where it does not occur at all [12].

In this paper, we analyze the capillary competition between random aperture-induced roughening and in-plane smoothing during immiscible phase displacements within rough-walled fractures. Through a perturbation analysis of the equation for capillary pressure, we find that the phase structure should depend critically on the ratio of two dimensionless parameters, C/δ, where δ is the coefficient of variation of the aperture field and C is the curvature number which weighs the mean influences of aperture induced and in-plane curvature. To characterize the displacement process, we consider the simple measure of phase structure given by the areal saturation at the end of displacement. Parametric numerical simulations using the MIP algorithm confirm that for small values of δ, phase structure and areal saturation are indeed uniquely determined by C/δ. However, for C/δ above ~ 0.5, areal saturation for wetting and nonwetting invasion fans apart and then converges to create an envelope whose width increases with δ. Such an envelope is explained by an accompanying divergence in the relative importance of roughening and smoothing processes at the back of the invasion front where phase entrapment occurs.

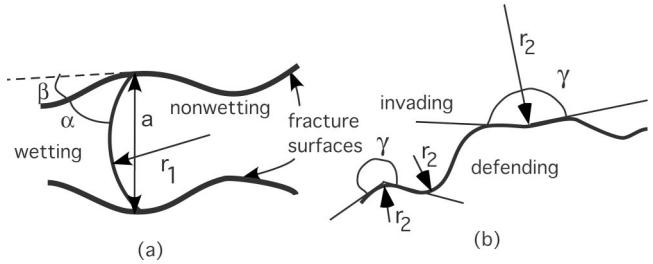

FIG. 1. Schematic of two fluid phases within a rough-walled fracture: (a) cross section defining the aperture-induced radius of curvature, r_1, local aperture a, contact angle α, and convergence-divergence angle β and (b) plan view (normal to fracture plane) defining the in-plane radius of curvature, r_2, and included angle γ (from invading phase).

PHASE INVASION MODEL AND PERTURBATION ANALYSIS

Quasistatic displacements within a horizontal, variable aperture fracture with negligible gravitational influence, are controlled by capillary forces acting at the interface between the two phases. The local capillary pressure (P_c) is represented in terms of the surface tension between the two fluids (T) and the interfacial curvature, using the Laplace-Young equation

$$P_c = T\left[\frac{1}{r_1} + \frac{1}{r_2}\right], \tag{1}$$

where r_1 and r_2 are the two principal radii of curvature. Assuming a well-defined contact angle (α) at fluid-fluid-solid contacts, one of the principal radii of curvature (r_1) will be normal to the fracture plane and may be written as

$$r_1 = -a/[2\cos(\alpha+\beta)], \tag{2}$$

where a is the local aperture (or gap) and β is the local convergence-divergence angle of the two fracture surfaces [see Fig. 1(a)]. The second principal radius of curvature (r_2) will be in the plane of the fracture and will evolve with the interface as it grows [see Fig. 1(b)]. After Glass *et al.* [12], we represent r_2 within a correlated random field as

$$r_2 = (\lambda/2)\tan(\gamma/2), \tag{3}$$

where λ is the spatial correlation length of the aperture field and γ is the included angle between two vectors that approximate the local interface from the invading fluid side [Fig. 1(b)]. This relation for r_2 yields appropriate values for γ at the end points of either 0° (0) or 180° (infinite) with a scaling by $\lambda/2$ taken as a characteristic in-plane radius of curvature within a spatially correlated field. MIP simulations that embody this approximation for r_2 have demonstrated agreement with physical experiments in variable aperture fractures [12]. We note that this representation of the physics [Eqs. (1), (2), and (3)] ignores wetting film flow and the accompanying snap-off of the nonwetting phase when it becomes encapsulated by wetting films (i.e., wetting phase coating the solid surfaces with nonwetting between).

Analysis of the capillary pressure equation illustrates the competition between aperture variation (r_1 term) and local in-plane curvature (r_2 term) in controlling interface movement. Let us first simplify for small β and for α near either 0 (wetting) or π (nonwetting). With $\langle a\rangle$ and a', respectively, denoting the mean aperture and deviations from the mean, substitution of $a=\langle a\rangle + a'$, and expansion of the r_1 term as a Taylor series yields

$$P_c = T\left[\mp\frac{2}{\langle a\rangle}\left(1 - \frac{a'}{\langle a\rangle} + \frac{a'^2}{\langle a\rangle^2} - \cdots\right) + \frac{2}{\lambda}\cot\left(\frac{\gamma}{2}\right)\right], \tag{4}$$

where the first term in the outer braces is $-$ for wetting and $+$ for nonwetting invasion. Recognizing that only perturbations away from the mean control the geometry of the interface and resulting phase structures, we can drop the term $2/\langle a\rangle$ and consider only perturbations in P_c:

$$P_c' = T\left[\mp\frac{2}{\langle a\rangle}\left(-\frac{a'}{\langle a\rangle} + \frac{a'^2}{\langle a\rangle^2} - \cdots\right) + \frac{2}{\lambda}\cot\left(\frac{\gamma}{2}\right)\right]. \tag{5}$$

Nondimensionalizing Eq. (5) and retaining terms only up to first order in a' we have

$$P_{c*}' = \mp\delta a_*' + C\cot\left(\frac{\gamma}{2}\right), \tag{6}$$

where

$$P_{c*}' = \frac{\langle a\rangle}{2T}P_c', \quad a_*' = \frac{a'}{\sigma_a}, \quad C = \frac{\langle a\rangle}{\lambda}.$$

In Eq. (6), σ_a is the standard deviation of a. Thus, interface movement and phase structure will be controlled by two dimensionless parameters: the coefficient of variation of the aperture field, δ, and the curvature number C. A measure of the strength of in-plane curvature relative to aperture-induced curvature is given by their ratio

$$\frac{C}{\delta} = \frac{\langle a\rangle^2}{\sigma_a\lambda}. \tag{7}$$

Based on this analysis, we expect that for small values of δ where the neglect of higher-order terms in Eq. (5) is justified, the dimensionless ratio C/δ will uniquely define the system behavior. For C/δ well below 1, aperture-induced curvature will dominate and the phase structure will be controlled by capillary fingering within the correlated field (small-scale correlated features on the order of 2λ and large-scale features that correspond to IP). As C/δ increases, capillary fingers will become wider than the correlation length as in-plane curvature begins to be important. For C/δ well above 1, the invading interface will become dominated by in-plane curvature and thus behave as in a smooth-walled Hele-Shaw cell with little or no entrapment of the defending phase. A subset of this behavior was observed by Glass *et al.* [12] for a fixed value of δ.

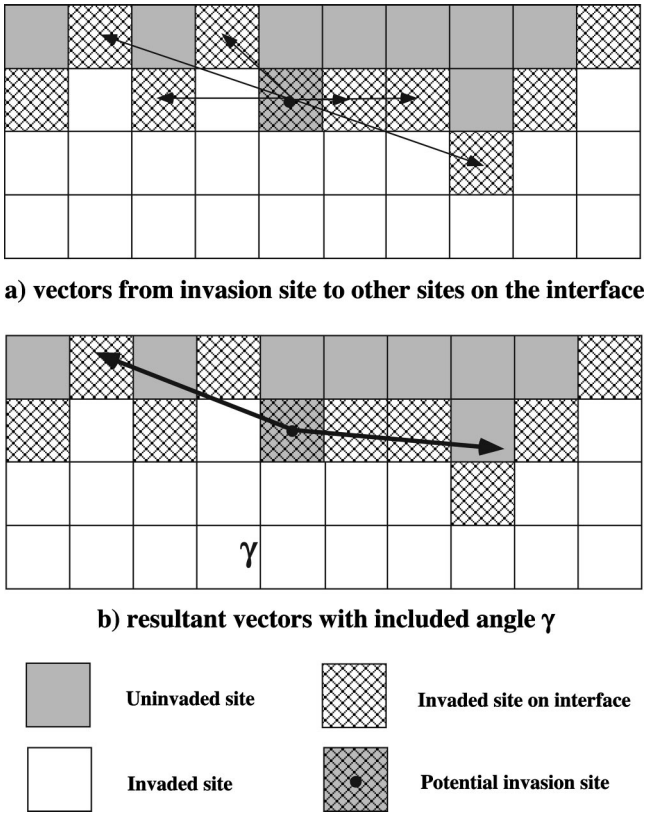

FIG. 2. Schematic for calculation of γ in Eq. (3): Looking downward onto a variable aperture field resolved as a checkerboard, blocks (sites) shown in white are filled with the invading fluid, hatched white are invaded sites on the active interface, and gray are filled with the defender fluid; the hatched gray block is the example site for which an invasion pressure including r_2 is calculated. (a) Vectors are found from the potential invasion site to sites up to a specified number of positions away both to the right and to the left along the interface. (b) An arithmetic average of unit vectors to the right and to the left of the potential invasion site defines the local average fluid interface and the included angle γ (from the invading phase) used for the calculation of r_2. Positions used for this calculation should be within a distance λ on each side of the potential invasion site. For illustrative purposes we have considered only three sites on either side of the potential invasion site in this figure. In practice the number of sites should not be less than 5 to adequately represent r_2 (minimum resolution of five sites per λ) [12].

PARAMETRIC STUDY DESIGN WITH THE MIP ALGORITHM

To consider the behavioral collapse for C/δ, we conducted a parametric study using the MIP algorithm [12] on computer-generated aperture fields. The aperture field is represented as a regular grid of sites with coordination 4 and Eq. (1) with Eqs. (2) and (3) is used to calculate P_c for potential invasion sites neighboring the growing interface. The included angle γ at each site is calculated as the angle between two mean vectors found by taking the arithmetic average of unit vectors from the potential invasion site to adjacent occupied sites in each direction along the interface within a distance λ (see Fig. 2). To resolve interfacial curvature adequately, the aperture field is resolved at a level of five grid blocks per λ [12]. An IP algorithm is implemented that invades the site along the interface with lowest P_c, after which P_c is recalculated for nearby sites to account for the change in local in-plane curvature.

Measurements of several fracture surfaces have suggested that they are self-affine with power function spectra for the individual fracture surfaces [16,17]. However, the aperture field corresponding to the gap between the surfaces only exhibits a power function spectrum above a low-wave-number cutoff corresponding to the mismatch length scale of the two surfaces [16,17]. Below the cutoff, the power spectrum approaches a constant value. To preserve these properties, we generated random aperture fields using the following form for the power spectrum of the aperture field:

$$G(k_x,k_y) \propto \frac{1}{(a+l^2k_x^2+l^2k_y^2)^n}. \tag{8}$$

In Eq. (6), k_x and k_y are the wave numbers corresponding to the x and y dimensions, n is an exponent in the range $1.0 < n < 1.5$ [16], and l is a cutoff length scale. This functional form of G yields a smooth transition from a power law behavior at large wave numbers ($|k| > 1/l$) to the cutoff value ($|k| < 1/l$) that results in random fields with well-behaved autocovariance functions (i.e., no oscillations as occur with an abrupt cutoff). We defined λ as the separation distance at which the autocorrelation reached a value of $1/e$.

With the power spectrum given by Eq. (6) we used a fast Fourier transform (FFT) algorithm to generate Gaussian random fields of size 1024×2048 grid blocks, with a mean of 0, variance of 1, and $n = 1.3$ [see the example of a 400×600 portion of an aperture field in Fig. 3(a)]. We then rescaled these fields to add a mean aperture and yield $\delta = 0.0625$, 0.125, and 0.25. At higher values of δ, contact areas where the aperture is zero introduce additional complication that will not be addressed here. Fourteen values of C were considered, beginning from 0, 0.002 09 with successive doubling up to 8.576. The invading phase was supplied across the entire edge of one short side of the random field while the defending phase was allowed to leave the field through the other three sides. Defending phase trapping was implemented and the simulation ended when all sites were either filled with invading phase or entrapped defending phase. Both wetting and nonwetting invasion simulations were carried out on six realizations of the random aperture field for each set of parameters (a total of 504 simulations).

SIMULATION RESULTS

Example portions of simulations from the middle of one aperture field realization are shown in Fig. 3 where entrapped phase is designated with black. The IP simulation [Fig. 3(b)] is significantly different from those that include in-plane curvature [Figs. 3(c)–3(h)]. For identical C/δ at a value of 0.536, different C and δ show nearly identical phase structures [compare Fig. 3(c) with Fig. 3(d)] and areal saturations ($S \sim 0.51$). However, at higher C/δ, we find some deviation for both wetting [compare Fig. 3(e) with Fig. 3(f)] and nonwetting [compare Fig. 3(g) with Fig. 3(h)] invasion as well

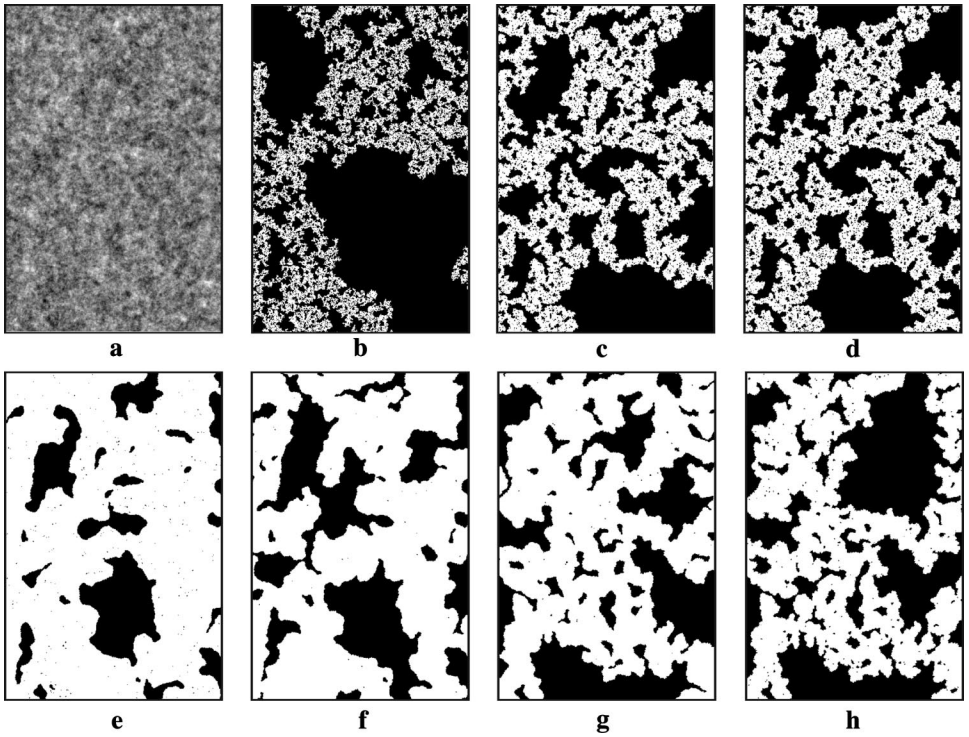

FIG. 3. Example phase invasion structures from 400×600 subsection of simulations: (a) Aperture field, grayscale depicts smaller apertures with darker shading; (b) wetting invasion, $C=0$, $\delta=0.0625$ (IP), $S\sim0.38$; (c) wetting invasion, $C=0.0335$, $\delta=0.0625$, $C/\delta=0.536$, $S\sim0.51$; (d) wetting invasion, $C=0.134$, $\delta=0.25$, $C/\delta=0.536$, $S\sim0.51$; (e) wetting invasion, $C=0.134$, $\delta=0.0625$, $C/\delta=2.144$, $S\sim0.74$; (f) wetting invasion, $C=0.536$, $\delta=0.25$, $C/\delta=2.144$, $S\sim0.81$; (g) nonwetting invasion, $C=0.134$, $\delta=0.0625$, $C/\delta=2.144$, $S\sim0.69$; and (h) nonwetting invasion, $C=0.536$, $\delta=0.25$, $C/\delta=2.144$, $S\sim0.63$. Black denotes regions where the defending phase is entrapped within the rough walled fracture.

as between wetting and nonwetting invasion.

The average areal saturation (S) computed from the six random field realizations is shown in Fig. 4 as a function of C, for different δ. The standard deviation in S across the realizations was typically small, ranging from 0.0075 (wetting) and 0.0179 (nonwetting) at $C=0$, to a maximum of about 0.02 at an intermediate value of C, and 0.0 at large values of C where there is no entrapment of the defending phase. As C increases at a fixed δ, S ranges from 0.37 at $C=0$ (IP limit) to 1.0 for large C. At a fixed value of C, increasing δ leads to a lower S, as expected. We also clearly see that away from the IP limit there is a difference between wetting and nonwetting invasions. For a given C and δ, nonwetting saturations are typically smaller than wetting saturations; the difference increases with C and then decreases again at high C, where $S=1$ for both cases. The C value at which wetting and nonwetting saturations start to deviate increases with δ, as does the C value at which deviations from the IP limit are noticeable. The latter is because for a larger value of δ, a larger value of C is needed to generate in-plane curvature effects strong enough to compete with the randomness in the aperture field.

When S is plotted as a function of C/δ (Fig. 5) there is a significant collapse in the behavior across different δ, with all cases practically coinciding for $C/\delta<0.268$. The deviation from the IP limit becomes noticeable at $C/\delta\sim0.134$. The point at which wetting and nonwetting saturations start to deviate beyond realization variability has also collapsed and corresponds to $C/\delta=0.536$ [see also Figs. 3(c) and 3(d)]. For $C/\delta>1$, there is further separation between the behavior for different δ, although there is less difference in S between the two smaller values of δ [Figs. 3(e)–3(g)]. Again, at large values of C/δ, S approaches 1.

DISCUSSION AND CONCLUSION

The foregoing results illustrate the competition between the smoothing influence of in-plane curvature (controlled by C) and the roughening influence of randomness in the aperture field (controlled by δ). At a fixed δ and for $C=0$, the phase structures are as in the IP algorithm within a correlated field and show significant phase entrapment. More compact phase structures and lower defending phase saturations are found as C increases, and for very large C, invasion is nearly planar with no entrapment of the defending phase. Our perturbation analysis suggests that a single parameter C/δ controls phase structures for small values of δ. The MIP model simulations validate the perturbation analysis, as evidenced by the significant collapse in the saturation results when plotted as a function of C/δ. However, the collapse is not perfect, and differences between the behavior in wetting and nonwetting invasion increase with C/δ to create an envelope where S first diverges above a C/δ of ~0.5 and then converges at higher values. We also find that the width of the envelope increases with δ.

The creation of the wetting versus nonwetting envelope is

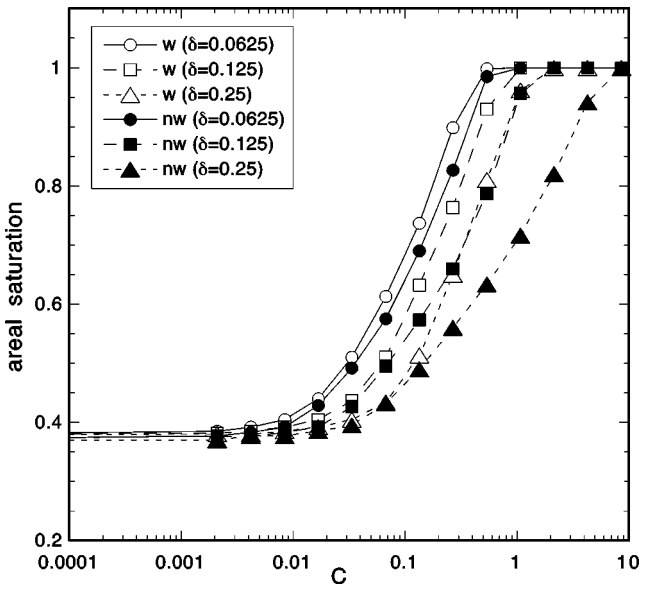

FIG. 4. Average areal saturation (S) computed from six random field realizations is shown as a function of C, for different δ. Wetting invasion (w) is denoted with open symbols and nonwetting (nw) with solid symbols.

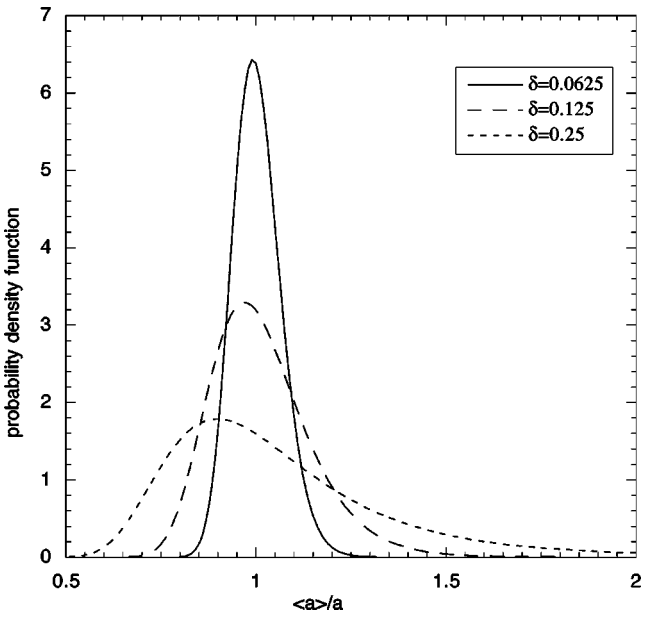

FIG. 6. Probability density function of normalized inverse aperture $\langle a \rangle / a$, for different values of the coefficient of variation (δ) of the aperture field.

explained by the nonlinear nature of aperture-induced capillary pressure (T/r_1 scales with $1/a$ rather than a). For a normally distributed a, $1/a$ has an asymmetric distribution (Fig. 6) with a long-tailed skew towards larger values of $1/a$ (smaller apertures). As a result, wetting and nonwetting invasions experience a much different distribution of $1/a$ as they invade from opposite ends of the asymmetric distribution. For wetting invasion, the distribution is wider at the leading edge of the displacement front (smaller a) and narrower at the back of the front (larger a), where entrapment predominantly occurs. Thus, in-plane curvature most effectively competes with aperture-induced curvature at the back of the front, leading to decreased entrapment and increased invading phase saturation. The opposite occurs at the back of the front for nonwetting invasion, where aperture-induced curvature is enhanced relative to in-plane curvature. The asymmetry in the $1/a$ distribution is very minor for $\delta = 0.0625$ and is amplified as δ increases. This explains the corresponding increase in the width of the wetting versus nonwetting envelope with increasing δ.

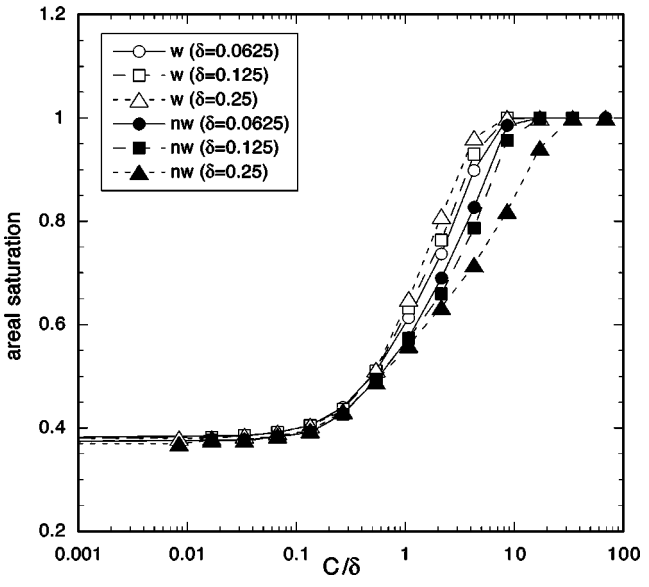

FIG. 5. Average areal saturation (S) computed from six random field realization is shown as a function of C/δ. Wetting invasion (w) is denoted with open symbols and nonwetting (nw) with solid symbols.

A general result from this work is the influence of random field amplitude (δ) on phase structure, a result not obtained from the standard IP algorithm. The influence of random field amplitude is expected to arise when another mechanism (in this case smoothing by in-plane curvature) competes with randomness to control interface movement. Although yet to be studied systematically, similar features may be expected in other problems modeled by a competing effect superimposed on an IP process. Examples include wetting in porous media where multiple-neck pore filling smoothes interfaces [6,7], density effects on buoyancy stabilized displacements in gravity fields [18] or centrifugal fields [19] as well as for buoyancy destabilized displacements [20,7,8], competition between correlated buoyancy and capillary thresholds in horizontal fractures [21], and the influence of viscous forces [22,13].

ACKNOWLEDGMENTS

This work was supported by the U.S. Department of Energy's Basic Energy Sciences Geoscience Research Program, under Contract Nos. DE-AC04-94AL85000 (Sandia National Laboratories), DE-FG03-96ER14590 (University of Colorado at Boulder), and W-7405-ENG-48 (Lawrence Livermore National Laboratory).

[1] R. Chandler, J. Koplik, K. Lerman, and J. F. Willemsen, J. Fluid Mech. **119**, 249 (1982).
[2] D. Wilkinson and J. F. Willemsen, J. Phys. A **16**, 3365 (1983).
[3] R. Lenormand, E. Toboul, and C. Zarcone, J. Fluid Mech. **189**, 165 (1988).
[4] R. Lenormand and C. Zarcone, Society of Petroleum Engineers No. 13264, in Proceedings of the 59th Annual Technical Conference of the SPE (1984).
[5] Y. Li and N. C. Wardlaw, J. Colloid Interface Sci. **109**, 473 (1986).
[6] M. J. Blunt and H. Scher, Phys. Rev. E **52**, 6387 (1995).
[7] R. J. Glass and L. Yarrington, Geoderma **70**, 231 (1996).
[8] R. J. Glass and L. Yarrington, Water Resour. Res. **39**, 1058 (2003).
[9] L. J. Pyrak-Nolte, D. Helgeson, G. M. Haley, and G. W. Morris, in *Rock Mechanics*, Proceedings of the 33rd U.S. Symposium, Rotterdam, The Netherlands, edited by J. R. Tillerson and W. R. Wawersik (A. A. Balkema, 1992).
[10] H. Amundsen, G. Wagner, U. Oxaal, P. Meakin, J. Feder, and T, Jossang, Water Resour. Res. **35**, 2619 (1999).
[11] G. Wagner, P. Meakin, J. Feder, and T. Jossang, Physica A **264**, 321 (1999).
[12] R. J. Glass, M. J. Nicholl, and L. Yarrington, Water Resour. Res. **34**, 3215 (1998).
[13] R. J. Hughes and M. J. Blunt, Adv. Water Resour. **24**, 409 (2001).
[14] R. J. Glass, H. Rajaram, M. J. Nicholl, and R. L. Detwiler, Curr. Opin. Colloid Interface Sci. **6**, 223 (2001).
[15] R. L. Detwiler, H. Rajaram, and R. J. Glass, Water Resour. Res. **37**, 3115 (2001).
[16] S. R. Brown, J. Geophys. Res. **100**, 5941 (1995).
[17] P. M. Adler and J. F. Thovert, *Fractures and Fracture Networks* (Kluwer, Boston, 1999).
[18] M. A. Ioannidis, I. Chatzis, and F. A. L. Dullien, Water Resour. Res. **32**, 3297 (1996).
[19] R. M. Holt, R. J. Glass, J. M. Sigda, and E. D. Mattson, Geophys. Res. Lett. **30**, 1692 (2003).
[20] P. Meakin, K.J. Maloy, J. Schmittbuhl, A. Hansen, and D. Bideau, Physica A **191**, 227 (1992).
[21] H. Auradou, A. Birovljev, V. Frette, J. Feder, and T. Jossang, Phys. Rev. E **60**, 7224 (1999).
[22] B. Xu, Y. C. Yortsos, and D. Salin, Phys. Rev. E **57**, 739 (1998).